MADRID
inter.noise 2019
June 16 - 19
NOISE CONTROL FOR A BETTER ENVIRONMENT

Noise Reduction Mechanism of Trailing Edge Blowing Using the Lattice-Boltzmann Method: Numerical and Experimental Analysis

Manegar, Farhan A.
Stahl, Kathrin
Carolus, Thomas H.
University of Siegen, Institute for Fluid- and Thermodynamics, 57068 Siegen, Germany

Binois, Rémy
Senvion GmbH, Überseering 10, 22297 Hamburg, Germany

ABSTRACT

Turbulent boundary layer trailing edge noise is a common problem in the wind turbine community. An active noise reduction method is the application of trailing edge blowing. A high fidelity simulation using the numerical Lattice Boltzmann method is used to identify an optimal trailing edge blowing configuration in terms of slot geometry and blowing jet velocity. The predicted aeroacoustic achievments are validated by experiments in the aeroacoustic wind tunnel (AWB) of the DLR in Braunschweig. To shed light on the underlying physical mechanisms, Lagrangian coherent structures are extracted from the numerical flow field data. They clearly show how trailing edge blowing shifts the acoustic energy from the low frequency region (turbulent boundary layer trailing edge noise) to the high frequency region (blunt trailing edge noise).

Keywords: Computational Aeroacoustics, wind turbine noise trailing edge noise
I-INCE Classification of Subject Number: 21

1. INTRODUCTION

Recent trends of diminishing fossil fuels has led to the increased installation of wind turbines, even in densely populated residential areas. Several researchers are currently developing methods to reduce noise sources in wind turbines, the most prominent probably being the flow induced turbulent boundary layer trailing edge noise (for simplicity referred to as TEN in this paper) [1]. Saw-tooth shaped serration add-ons at the trailing edge (TE) are the most common noise reduction technique that wind turbine manufacturers are implementing. Other potential noise mitigating methods are also investigated, like the design of a boundary-layer suction system [2], porous trailing edges [3] and blade shape optimization [4].

This paper focuses on the active trailing edge blowing (TEB). The naive idea of TEB is “blowing away” the turbulent structures within the boundary layer before they are scattered at the trailing edge due to its discontinuity. This scattering of the turbulent structures is one of the major causes of flow induced broadband noise from an airfoil. TEB has been intensively investigated e.g. by Gerhard et al [5]. He reported that blow-

ing through a small slot at a region close to TE on suction side, constituting 50% of the incoming flow velocity, can reduce TEN by around 3 dB. The investigations were carried out at a Reynolds number $Re = 3.5 \cdot 10^5$ for different type of airfoils such as NACA0015, S834 and DU93. In this study, the same technique of Gerhard et al is used but on a much larger scale, i.e. at $Re = 1.2 \cdot 10^6$, and exclusively applied to a DU93W210 airfoil section. Following parameters are relevant for TEB: The chord-wise position and width of the blowing slot and the mass flow rate (i.e. the velocity) of the blowing jet. The Lattice-Boltzmann-method (LBM) is used as a computational aero-acoustics tool for studying the influence of these parameters and to design a measurement matrix for a measurement campaign conducted at the aeroacoustic wind tunnel (AWB) of the DLR in Braunschweig. The TEB configuration which promised the best noise reduction has been chosen and further analysed in this paper to understand the physical mechanism of TEB and its effects on far-field noise.

2. COMPUTATIONAL METHOD

2.1 FLOW SOLVER

Traditional CFD methods solve the partial differential NAVIER-STOKES (N-S) equations, whereas LBM uses the discrete BOLTZMANN equations to simulate the flow at a kinetic level [6]. Particle distribution functions (PDF), which are defined as the number density of molecules at position x and speed u at a time t, are used by the BOLTZMANN equations to capture the kinetic behaviour of particles in the lattice world. LBM is inherently time-dependent. Macroscopic fluid properties like density and velocity are derived from these PDFs. Such a discretization strategy leads to conservation of mass, momentum and energy. Readers are referred to [7] for elaborate explanation of a LBM flow solver.

In this study, a turbulence model called very large-eddy simulation (VLES) is used. It consists of a two-equation k-ε renormalization group (RNG) [8]. These two equations are further modified to incorporate a swirl correction factor [9]. This enables the resolution of unsteady large-scale vortices. In high Reynolds number cases, a wall function is used to model the effect of the boundary layer on the rest of the flow because fully resolving the near wall region is computationally expensive. Hence, the cell closest to a surface is assumed to obey the law of the wall. A hybrid wall function smoothly transitions from a turbulent wall function (i.e. a logarithmic profile) at high y^+ values (above 35) to a viscous wall function (i.e. a linear profile) at low y^+ values (below 5). Along with the velocity profiles, this hybrid wall function is coupled with a wall model pressure gradient extension to account for the effects of favourable and adverse pressure gradient on the near-wall boundary layer profile [10].

All LBM simulations were carried out employing the commercial software 3DS-Simulia™ PowerFLOW, version 5.4b.

2.2 NOISE COMPUTATION

The advantage of using a LBM rather a N-S method is that it allows the direct computation of the radiated sound in the far-field. In this study only a segment of the experimentally measured span is simulated. The TEN, computed directly at monitoring points corresponding to microphone positions, needs to be corrected for the contributions from mirrored coherent images due to cyclic boundary conditions in the segmented span. Hence a more robust method is chosen, where time-dependent blade surface pressure fluctuations are fed into the acoustic analogy, namely Ffowcs Williams and Hawkings (FWH) [11, 12].

Since the experiment and simulation are potentially associated with different source-to-listener distances R, different span lengths b, and different Mach numbers M, the far-field L_{Spp} is scaled - as in many TEN problems, assuming a non-compact noise source [12] – to a reference radius of R_c = 1 m, a reference Mach number M_c = 1 and a reference span of b_c = 1 m via

$$L_{S_{pp},scaled} = L_{S_{pp}} + 10\log_{10}\left[\left(\frac{R}{R_c}\right)^2 \Big/ \left(\left(\frac{b}{b_c}\right)\left(\frac{M}{M_c}\right)^5\right)\right]. \quad (1)$$

2.3 LAGRANGIAN COHERENT STRUCTURES

It is a well-known challenge to segregate the turbulent fluctuations from acoustic fluctuations in the near-field, in other words, to spot the acoustic sources amidst the turbulent flow field. The difficulty arises due to the fact that the acoustic fluctuations have very less energy compared to the turbulent fluctuations. A reasonable first step would be to identify the vortex dynamics and flow behaviour, which eventually leads to the production of sound. Visualizing vorticity generated in the Eulerian frame of references provides limited information to understand the vortex behaviour. A much deeper insight is acquired using the Lagrangian frame of reference, where the flow behaviour is studied based on their trajectories in phase time and space [13].

In this study, Lagrangian Coherent Structures (LCS) are derived as in Shadden et al [13]. Ridges of finite-time Lyapunov exponent (FTLE), which describe how many flow particles separate after a given interval of time, are used to define LCS. In other words, as described by Shadden et al [13], imagine a pair of particles being advected in the flow; FTLE is then the finite time average of the maximum expansion rate of the pair. The methodology for computing FTLE fields from simulation data is as follows: Only the flow field in the vicinity of TE along mid span is evaluated. Consider a point x in the flow field at initial time t_0. After a time interval T, the point, when gets advected, moves to $\phi_{t0}^{t0+T}(x)$, where ϕ_{t0}^{t0+T} is the flow map which takes points from t_0 to their positions at time t. Now imagine an unsettled point y which is arbitrarily oriented and is defined as $y = x + \delta x(0)$. After the same time interval T, this unsettled point has now evolved in the flow map as

$$\delta x(T) = \phi_{t0}^{t0+T}(y) - \phi_{t0}^{t0+T}(x). \quad (2)$$

After applying the Landau notation to eq. (2), one gets $\delta\mathbf{x}(T)$ as a function of the finite time version of the Cauchy-Green deformation tensor:

$$\Delta = \frac{d\phi_{t0}^{t0+T}(x)^*}{dx}\frac{d\phi_{t0}^{t0+T}(x)}{dx} \quad (3)$$

To get the maximum stretching, the equations are rewritten by choosing $\delta x(0)$ in a way that it is aligned with the eigenvector associated with the maximum eigenvalue of Δ. Finally the largest FTLE is expressed as

$$\sigma_{t0}^{T}(X) = \frac{1}{|T|} ln\sqrt{\lambda_{max}(\Delta)} \quad (4)$$

which corresponds to the point x at time t_0. In general one can use backward time integration for locating attracting LCS and forward-time integration for locating repelling LCS. Eq. (4) uses absolute values of the integration time T, which allows both forward and backward-integration. It has to be mentioned that forward-integration has been used in this study.

3. CASE-SETUP

The main coordinate system is centred at the TE of the airfoil segment, Fig. 1. The two-dimensional airfoil DU93W210 extruded in the Z-direction, here named 2.5 D, has been investigated. It has a chord length c = 300 mm and a span of 800 mm at the experiment. Simulations are conducted only for a segment of this span (10% c) with periodic conditions in the Z-axis to reduce computational cost. Zig-Zag shaped tripping bands are positioned at 2% c and 5% c downstream of the leading edge on the suction and pressure side, respectively. The thickness of the trip on either side is set such that at least 8 finest voxels resolve the trip.

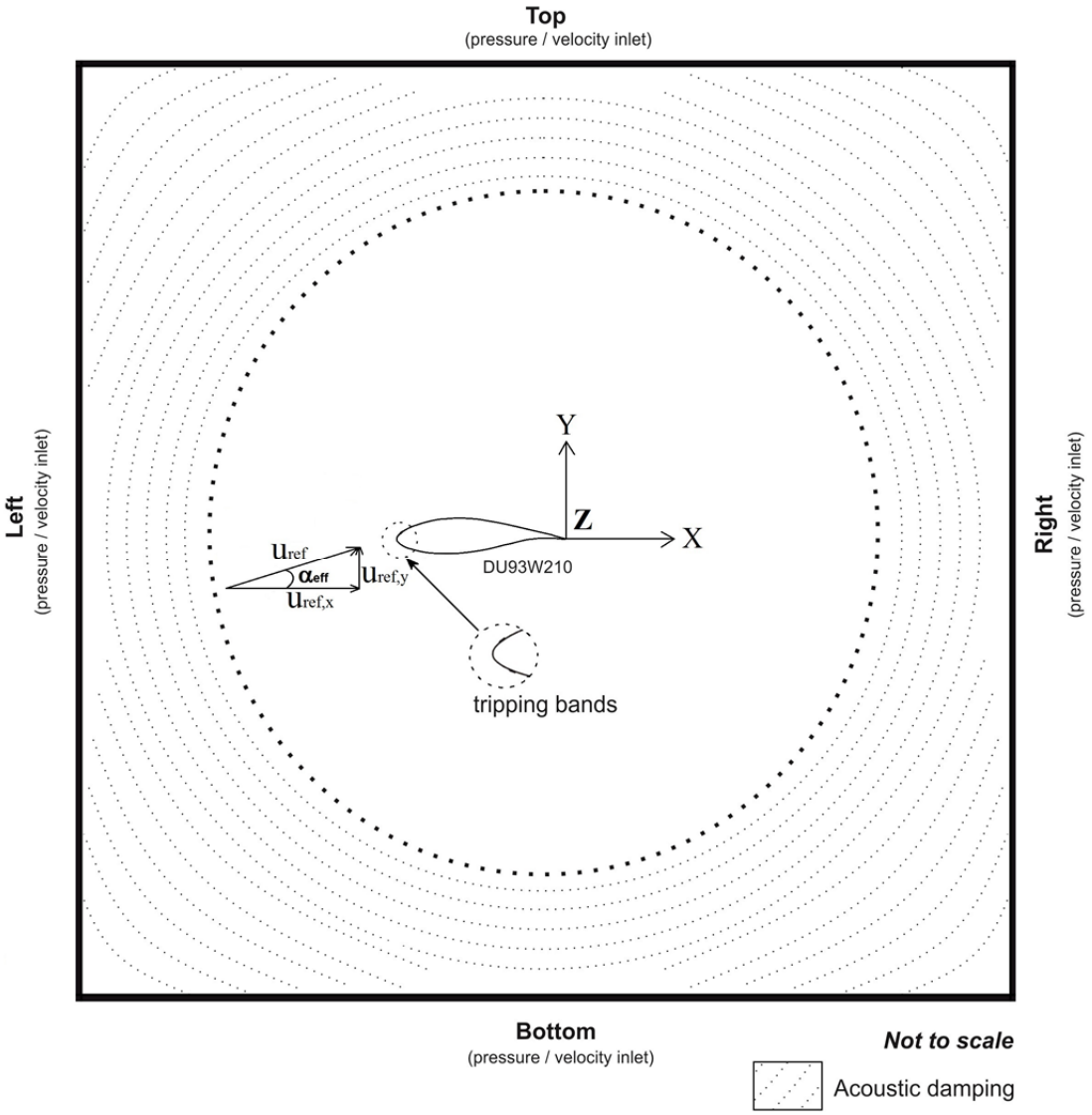

Figure 1. Schematic of airfoil segment and simulation domain in LBM (not to scale)

Simulations are conducted with a free inflow of u_{ref} = 60 m/s which leads to a chord based Reynolds number of $1.2 \cdot 10^6$. The effective angle of attack is α_{eff} = 3.5º. In the *experiments*, the 2.5 D model is tested with a geometric angle of attack α_{geom} = 8º. This compensates for the wind tunnel effect and lift loss associated with the confined jet. (α_{geom} = 8º has been found by comparing experimentally measured pressure distributions with the XFOIL-predicted [14] at α_{eff} = 3.5º.)

Fig. 1 also shows a schematic of the simulation domain (not to scale).The numerical grid consists of several zones of variable resolution (VR). Each VR zone con-

sists of cubical volume cells called voxels. The size of voxels increases by a factor of two in adjacent VR zones. The simulation case is setup with 9 VR zones, with the finest cell close to the blade surface being 5.86e-05 m and the coarsest cell being 0.015 m. The simulation domain is 100 *c* long in the X and Y-axis. The blade is placed at the centre of the simulation domain. This type of discretization results in $240 \cdot 10^6$ voxels. The smallest time step is 9.742e-08 s.

Boundary conditions are provided in terms of velocity and pressure at all four boundaries of the simulation domain. The fluid region outside an imaginary cylinder of radius 33 *c* drawn around the blade is provided with an acoustic sponge medium, whose viscosity increases exponentially as it reaches the simulation domain boundaries. This helps to damp the acoustic reflections. The simulated Mach number ($M = 0.175$) is chosen to be the same as in the experiment, such that the acoustic waves propagate at the same speed as they do in the experiment.

Even though the active TEB at the experiment has been realised using a very elaborated TEB geometry (explained in section 4), a simplification is applied in the simulation case: Essentially, the blowing jet with its direction and velocity is a boundary condition as shown in Fig. 2.

All the unsteady simulation results shown in this study are evaluated with a sampling rate $f_s = 20$ kHz and are recorded for 20 flow passes (c/u_{ref}). To calculate one single flow pass takes 1400 CPU hours on an Intel Xeon Haswell EP E5-2630v3 platform with 180 cores.

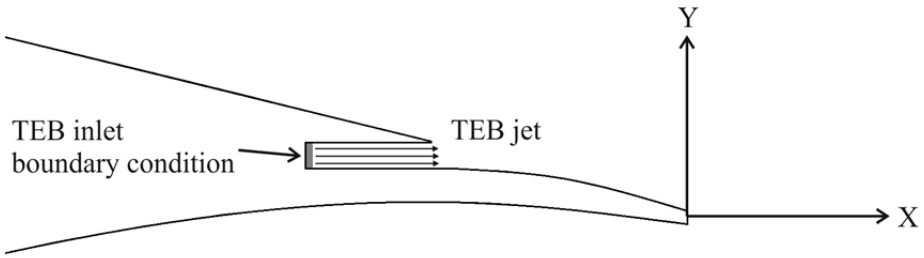

Figure 2. Schematic of active TEB realisation in LBM

4. EXPERIMENTAL DETAILS

The experiments were conducted at the DLR-operated Aeroacoustic Wind Tunnel Braunschweig - AWB. It is an open-jet low noise wind tunnel with a rectangular nozzle dimension of 0.8 m x 1.2 m. Since it is an open wind tunnel, direct measurement of acoustics is very challenging due to an unfavourable signal to noise ratio (SNR). However, the wind tunnel is equipped with two sophisticated sound capturing systems, an acoustic mirror and an acoustic microphone array.

The acoustic mirror is placed outside of the wind tunnel jet below the pressure side of the airfoil segment and can be moved up- and downstream in small steps, Fig. 3 (right). It has a highly directional characteristic and is a very effective instrument to focus on TEN, especially with such low-noise TE modifications. Due to the dimensions of the acoustic mirror only signals with frequencies > 1000 Hz can be resolved reliably. The measured spectrum using the acoustic mirror is corrected for sound wave convection, extraneous wind-tunnel noise sources, system response function (effective spatial resolution and gain) and source distribution. By doing so, the absolute TEN level is provided and the values are available in 3rd octave band frequency bins.

In the experiment, the surface pressure fluctuations on the suction side of the airfoil in the vicinity of the trailing edge were measured by a special probe microphone

(1/4″ condenser microphone with a 50 mm long probe tube - Brüel & Kjær type 4182) as shown in Fig. 3 (left bottom). The probe microphone values have been corrected for the non-flat frequency response in the range of 20 Hz to 10 kHz using the frequency response curve provided by the manufacturer. The probe is placed at X/c = -0.07.

The spectral power density (S_{pp}) is obtained using *pwelch* function in Matlab™ with a Hanning window and 50% overlap. Its level is then computed relative to a reference sound pressure $p_0 = 2 \cdot 10^{-5}$ Pa. Δf_0 is set to 1 Hz. L_{Spp} is scaled in the the same manner as in eq. (1).

The active TEB has been realised with a system consisting of a air supplying fan, sound attenuator, Venturimeter and tubes (Fig. 3 – left top). With the help of the Venturimeter the flow rate has been set for the desired blowing jet velocity. The blade has an inner chamber from where the flow is fed into the blowing slot. The cross-section in the chamber decreases with the distance from the air inlet to deliver a uniform flow rate along the spanwise slot, as shown in Fig. 4 (left). Honeycomb flow straighteners at the slot entrance are installed to reduce the turbulence intensity of the blowing jet.

The results and validation of the parametric study is not shown in this paper. The acoustically favorable TEB configuration was found to have a blowing slot positioned at 90% c with a thickness of the slot of 1% c. The blowing jet has a velocity of 70% of u_{ref}. Fig. 5 shows a schematic of this TEB configuration. From now on in this paper, this TEB configuration is referred to as TEB and the solid TE is referred to as reference and investigated further.

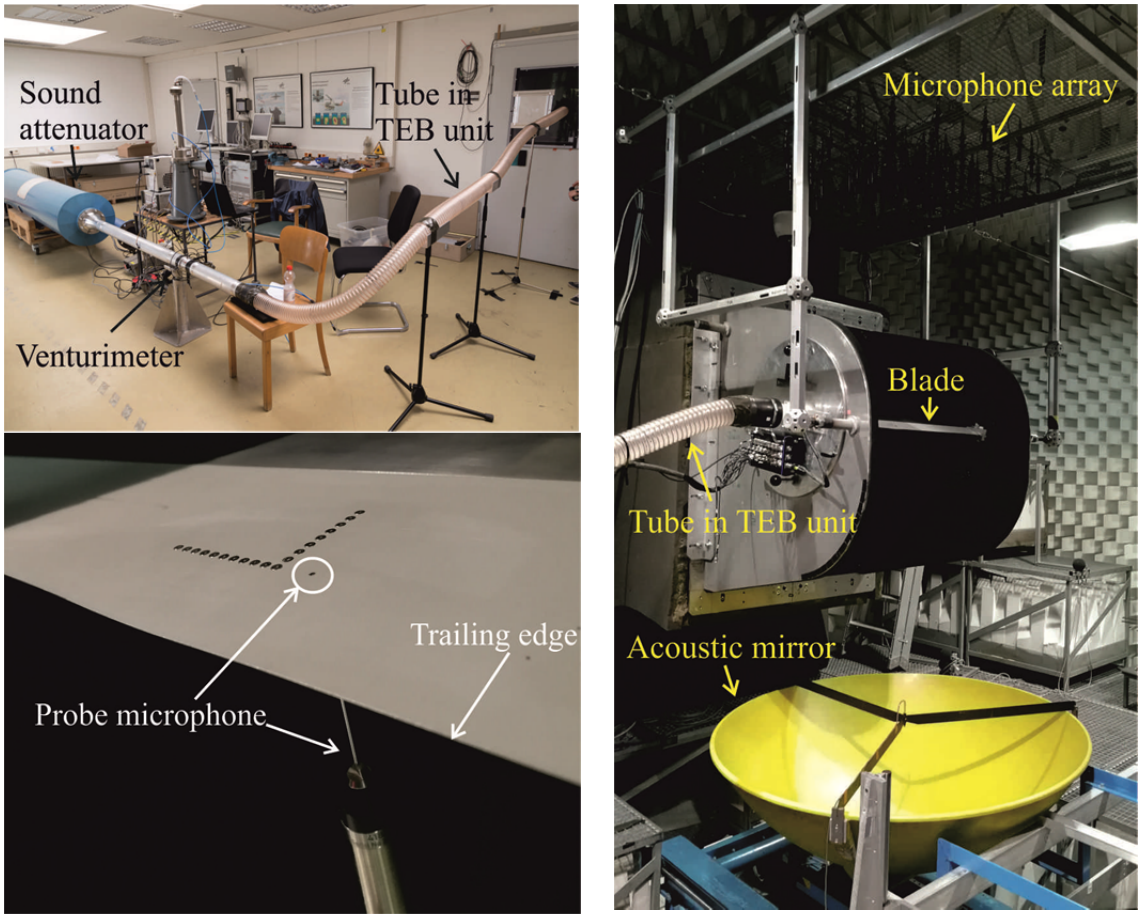

Figure 3. TEB unit setup outside wind tunnel (left top). Probe microphone used to measure surface pressure fluctuations (left bottom). Blade installed at the wind tunnel nozzle and acoustic measurement systems (right)

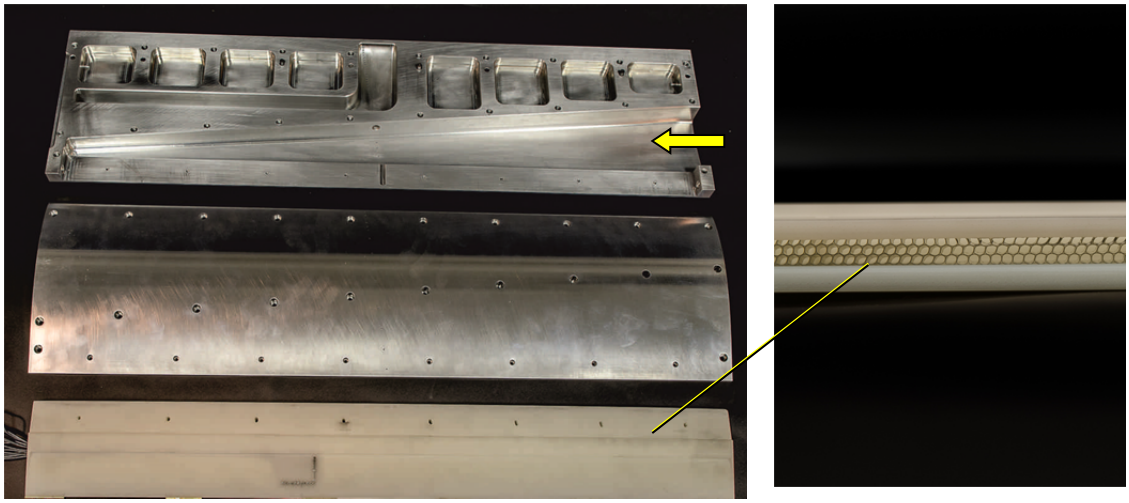

Figure 4. Dismantled Blade showing inner chamber used to realise TEB (left). Honeycomb flow straighteners installed at the entrance of the blowing slot (right)

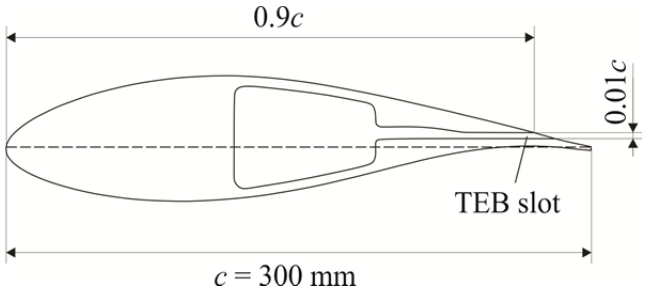

Figure 5. Schematic of best TEB configuration (from the results of a parametric study)

5. RESULTS

5.1 VALIDATION

The footprint of the turbulent boundary layer is the fluctuating surface pressure which acts as producer of trailing edge sound. Hence, the very first quantity of interest is the time dependant surface pressure fluctuation in the vicinity of the TE. Exemplarily, for the reference case, Fig. 6 depicts both, the spectrum of the LBM-predicted and measured surface pressure at X/*c* = - 0.07. The match between experiment and simulation is very good up to 2 kHz. For higher frequencies the simulation tends to slightly over predict the experimental data.

Fig. 7 shows the far-field noise spectra comparison between experiment and LBM for reference and TEB case. The agreement between experiment and LBM is remarkable. There are few disagreements, for instance the simulation under predicts in the case of TEB at 1 kHz by 3 dB. But importantly LBM can exactly predict the high frequency hump around 5000 Hz in the TEB configuration. In the next section, the physical mechanism behind this high frequency hump is analysed.

5.2 PHYSICAL MECHANISM

Boundary layer quantities

TEB mainly affects the turbulent boundary layer in the vicinity of the TE. In this section, the numerically predicted boundary layer development in the vicinity of TE is compared between the reference and TEB configurations. Fig. 8 (right) shows the

boundary layer development on the suction side of the blade in terms of boundary layer displacement thickness δ^*. The values are calculated at the red lines shown in Fig. 8 (left). δ^* is also calculated using XFOIL for the corresponding flow conditions and is plotted only for the reference configuration. δ^* of TEB configuration develops more densely compared to the reference, until TEB is applied. After that, the δ^* reduces drastically owing to the fact that the turbulence has been "blown away".

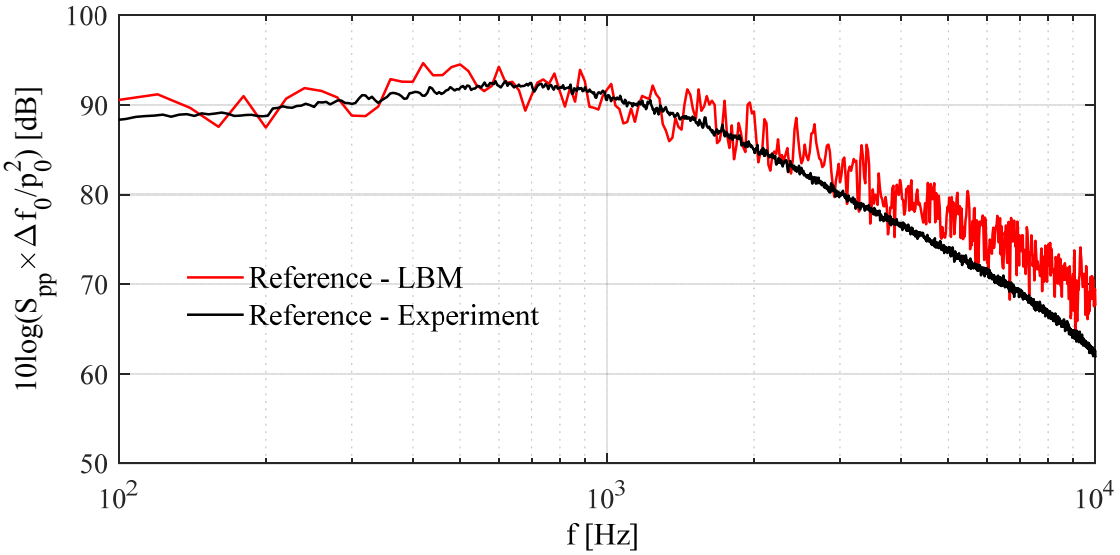

Figure 6. Surface pressure fluctuations on the suction side at X/c = - 0.07; reference case only, i.e. without TEB

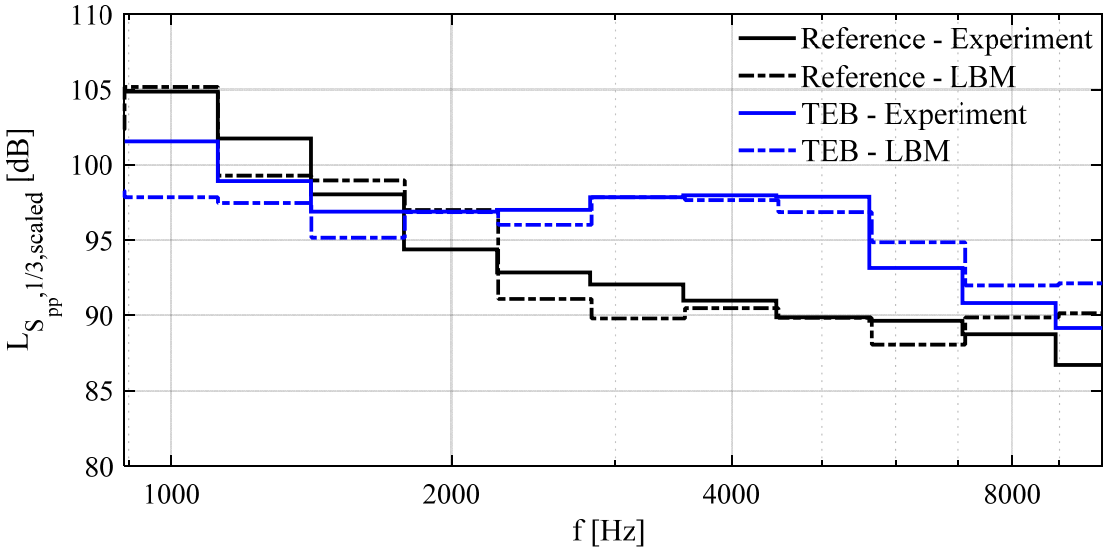

Figure 7. Far-field noise spectra measured with acoustic mirror at AWB – Reference vs. LBM

To look further into the velocity and turbulence quantities at TE, the velocity profile and root mean square (rms) of the velocities are shown in Fig. 9. The velocity profiles in the left figure shows that a very thin boundary layer is developing at the vicinity of TE in the case of TEB. It is known from literature that the trailing edge thickness of blade should be thin enough to avoid the generation of blunt trailing edge noise (BTEN), which appears at high frequencies as a narrow band peak. From Fig. 9

(right), it is evident that most of the turbulence is now shifted away from TE wall in the case of TEB. It then can be speculated that the new very thin boundary layer, starting at the slot then induces BTEN. The evalutation of the associated Lagrangian Coherent Structures (LCS) support this hypothesis.

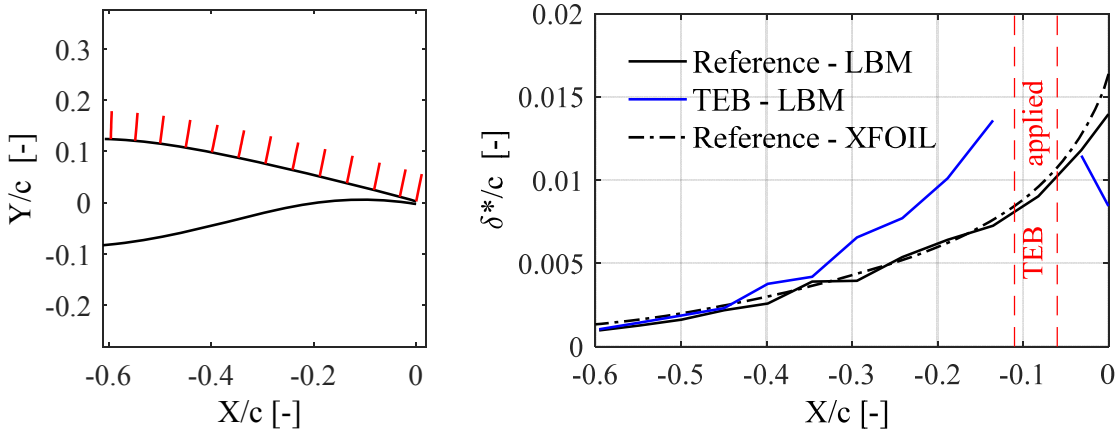

Figure 8. Locations where boundary layer displacement thickness is calculated – red lines (left), boundary layer displacement thickness comparison – LBM (right)

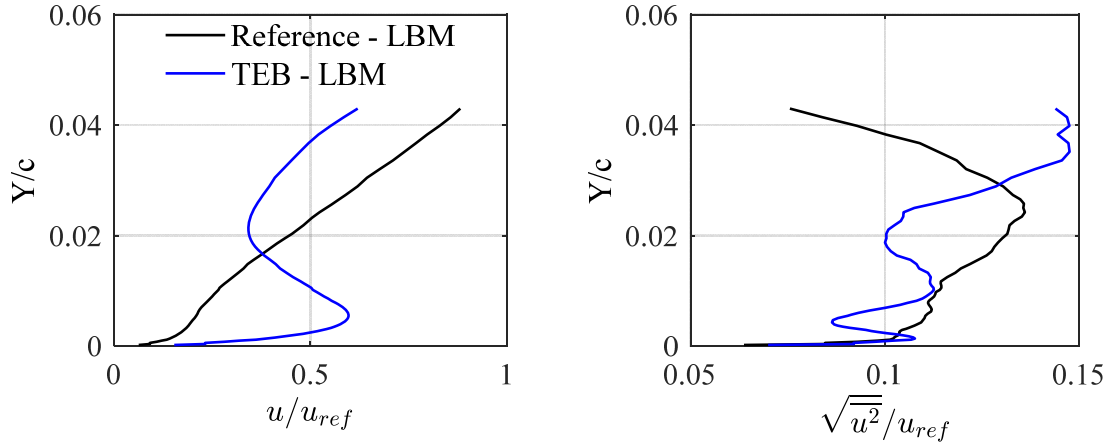

Figure 9. Velocity profile at TE – LBM (left), root mean square values of velocities at TE – LBM (right)

Lagrangian Coherence Structures

LCS are extracted from the flow field data in the vicinity of TE as described in section 2.3. It is always not so straight forward to set the integration time for calculating the FTLE fields. After a few trials, an integration time comprising of 15 samples has been chosen, as this resolves sufficient details of the LCS structures. The time interval between each sample is 50 µs, at which the velocity data is available.

LCS are defined as ridges on the finite-time Lyapunov exponent (FTLE) field, these ridges could be identified based on the geometrical definitions described by Shadden et al [13]. However, LCS are also visually recognisable and is a much easier way to plot the ridges. In Fig. 10, the LCS, which are defined as more than 60% of the maximum FTLE field, are shown. The stable manifolds revealing repelling LCS are clearly visible. The structures basically show how the energy is being advected and where the mixing happens. In the TEB configuration, one can see that the blowing jet temporarily stops the structures which are trying to advect and hence enhances mixing among them (refer the white ellipse in Fig. 10 right). Hence the big structures are then broken down,

which is a possible explanation for achieving 3 dB noise reduction at 1 kHz. On the other hand, the small boundary layer developing in the very close vicinity of TE (X/*c* = -0.05 to X/*c* = 0) is then adding more energy to the LCS structure at the TE (refer the blue circle in Fig. 10 right). This generates the necessary sources for the BTEN which appears in the high frequency (5 kHz). This is all in contrast to the reference case shown in Fig. 10 left, where those structures are non-existent. Hence, it is concluded that these different vortex structures obtained by TEB, result in the change of far-field acoustic as seen in Fig. 7.

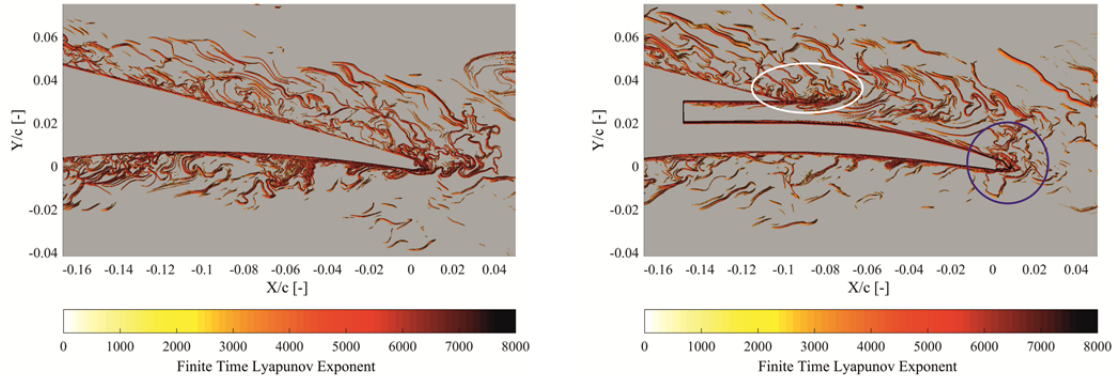

Figure 10. LCS (more than 60 % of maximum FTLE field), reference (left) and TEB (right)

6. CONCLUSIONS

The best active TEB configuration from a parametric study (conducted using LBM and experiment) is analysed in this paper. This TEB configuration provides 3 dB noise reduction at 1 kHz. Additionally, there is an unexpected high frequency hump around 5 kHz with a 7 dB noise increase. LBM results are first validated using the experimental results, where a very good agreement between LBM and experiment is seen for both near field surface pressure fluctuations and far-field acoustics.

The flow-field recorded in LBM is further analysed to understand the physical mechanism of TEB. The boundary layer development on the suction side and the velocity profile at TE show that in the case of TEB a small boundary layer starts developing very close to TE. The rms values of the velocity fluctuations at TE shows that turbulent energy is blown away from the TE (wall normal direction).

Stable manifolds revealing repelling LCS show that the blowing jet blocks the coherent structures from being convected further downstream and enhances mixing among the large scale structures. This explains the 3 dB noise reduction at 1 kHz. The small boundary layer that develops very close to TE adds to the stable LCS structure at the TE. This is speculated to induce BTEN and result in the noise increase of around 5 kHz. In future studies, further evaluation of LCS ridges will be carried out to check the rate of flux flowing through the LCS.

7. ACKNOWLEDGEMENTS

Financial support for this work was partly provided by the Federal Ministry for Economic Affairs and Energy of Germany (BMWi) within the project RENEW (FKZ 0325838B).

We acknowledge gratefully 3DS-Simulia™ for providing the licenses and technical assistance to carry out the LBM simulations. We also acknowledge the staff at the

aeroacoustic wind tunnel (AWB) of the DLR in Braunschweig for their support during the measurement campaign.

8. REFERENCES

1. S. Oerlemans, P. Sijtsma and B. Méndez López , *"Location and quantification of noise sources on a wind turbine"*, Journal of Sound and Vibration, Volume 299, Issues 4–5 (2007)
2. B. Arnold, Th. Lutz and E. Krämer, *"Design of a boundary-layer suction system for turbulent trailing-edge noise reduction of wind turbines"*, Renewable Energy, Volume 123, Pages 249-262 (2018)
3. T. Geyer and E.Sarradj, *"Trailing Edge Noise of Partially Porous Airfoils"*, 20th AIAA/CEAS Aeroacoustics Conference Atlanta, GA (2014)
4. S. Oerlemans, M. Fisher, T. Maeder and K. Kögler, *"Reduction of Wind Turbine Noise Using Optimized Airfoils And Trailing-Edge Serrations"*, 14th AIAA/CEAS Aeroacoustics Conference (29th AIAA Aeroacoustics Conference), Vancouver, British Columbia, Canada (2008)
5. T Gerhard, S Erbslöh and T Carolus, *"Reduction of airfoil trailing edge noise by trailing edge blowing"*, Journal of Physics: Conference Series, Volume 524, conference 1 (2014)
6. S. Succi, *"The Lattice Boltzmann Equation for fluid dynamics and beyond"*, Oxford Univesity Press, Oxford (2001)
7. S. Chen and G. D. Doolen, *"Lattice Boltzmann Method for Fluid Flows"*, Annual Review of Fluid Mechanics, Vol. 30, pp. 329-364 (1998)
8. V. Yakhot and S. Orszag, *"Renormalization group analysis of turbulence. I. basic theory"*, Jorunal of Scientific Computing, 1: 3-51 (1986)
9. H. Chen, S. Kandasamy, S. Orszag, R. Shock, S. Succi and V. Yakhot, *"Extended Boltzmann kinetic equation for turbulent flows"*, Science, 301: 307-314 (2003)
10. R. Kotapati, R. Shock and H. Chen, *"Lattice-Boltzmann simulations of flows over backward-facing inclined steps"*, International Journal of Modern Physics C, 25: 1340021 (2014)
11. G. Bres, F. Perot and D. Freed, *"A Ffowcs Williams-Hawkings solver for Lattice-Boltzmann based computational aeroacoustics"*, 16th AIAA/CEAS Aeroacoustic Conference, Stockholm, Sweden (2010)
12. W. C. P. van der Velden, A. H. van Zuijlen and D. Ragni, *"Flow topology and noise emission around straight,serrated and slitted trailing edges using the Lattice Boltzmann methodology"*, 22nd AIAA/CEAS Aeroacoustics Conference, Lyon, France (2016)
13. S. C. Shadden, F. Lekien and J. E. Marsden, *"Definition and properties of Lagrangian coherent structures from finite-time Lyapunov exponents in two-dimensional aperiodic flows"*, Physica D 212, 271–304 (2005)
14. M. Drela and H. Youngren, *"XFOIL 6.94 User Guide"*, Technical Report, Massachusetts Institute of Technology, Cambridge, MA (2001)